Influence of molecular motors on the motion of particles in viscoelastic media

Sebastián Bouzat*

Consejo Nacional de Investigaciones Científicas y Técnicas, Centro Atómico Bariloche (CNEA), (8400) Bariloche, Río Negro, Argentina

(Received 19 December 2013; revised manuscript received 29 April 2014; published 16 June 2014)

We study theoretically and by numerical simulations the motion of particles driven by molecular motors in a viscoelastic medium representing the cell cytoplasm. For this, we consider a generalized Langevin equation coupled to a stochastic stepping dynamics for the motors that takes into account the action of each motor separately. In the absence of motors, the model produces subdiffusive motion of particles characterized by a power-law scaling of the mean square displacement versus the lag time as t^{α}, with $0 < \alpha < 1$, similar to that observed in cells. Our results show how the action of the motors can induce a transition to a superdiffusive regime at large lag times with the characteristics of those found in experiments reported in the literature. We also show that at small lag times, the motors can act as static crosslinkers that slow down the natural subdiffusive transport. An analysis of previously reported experimental data in the relevant time scales provides evidence of this phenomenon. Finally, we study the effect of a harmonic potential representing an optical trap, and we show a way to approach to a macroscopic description of the active transport in cells. This last point stresses the relevance of the molecular motors for generating not only directed motion to specific targets, but also fast diffusivelike random motion.

DOI: 10.1103/PhysRevE.89.062707 PACS number(s): 87.16.Uv, 87.16.Nn, 05.40.−a

I. INTRODUCTION

Active cargo transport mediated by molecular motors (also called motor proteins) is essential for cell functioning. Two main mechanisms can be distinguished which are ubiquitous in eukaryotic cells, namely, microtubule-based transport [1,2] and actin-based transport [1,3]. Microtubules and actin filaments are polymeric structures along which the molecular motors can translocate (or *walk*) carrying different types of cargos such as vesicles, lipid droplets, mitochondria, and organelles with pigments [1–3]. For this, the motors use energy taken from the hydrolysis of the adenosine triphosphate (ATP) [1]. Both microtubules and actin filaments are polar structures with well defined plus and minus ends, so that the spatial symmetry is broken on each filament and the motors can *recognize* the appropriate direction of motion. Transport along microtubules is mediated by kinesin motors, which walk to the plus end, and dynein motors, which walk in the opposite sense [2]. Meanwhile, actin-based transport is mediated by different types of myosin motors [1,3]. For instance, myosin V walks to the plus end of the actin filaments (also called the barbed end) while myosin VI walks to the minus end [1,3,4]. Inside cells, the microtubules are mostly oriented with their minus ends close to the nucleus and their plus ends close to the cell membrane, while actin filaments are distributed in a rather random way generating the actin network [1].

The cell cytoplasm is a complex crowded environment with macromolecules embedded and also semiflexible polymers of different sizes, including the mentioned actin network and the microtubules, which together with the intermediate filaments constitute the cytoskeleton [1,5]. Due to this, the cytoplasm shows both viscous and elastic responses to deformations or movement of particles inside and, thus, it has the properties of a viscoelastic medium [5,6]. The rheological properties of a viscoleastic medium are closely related to the mean square displacement (MSD) associated to the thermal motion of the particles embedded on it [5]. In fact, the determination of the MSD of the particles as a function of the lag time (i.e., the time between two measurements of the particle position) allows us to estimate the complex modulus $G(\omega)$ of the medium [5,7], which characterizes both its viscous and elastic properties. Depending on the behavior of the MSD as a function of the lag time t, the motion of particles is classified as diffusive (MSD $\sim t$), subdiffusive (MSD $\sim t^{\beta}$ with $0 < \beta < 1$), superdiffusive (MSD $\sim t^{\beta}$ with $1 < \beta < 2$), or ballistic (MSD $\sim t^2$). Due to the viscoelastic properties of the cytoplasm, the thermal motion inside cells in the absence of active transport is normally subdiffusive at small and intermediate lag times [5,8], and slowly diffusive at large lag times [5]. Meanwhile, the action of molecular motors can generate ballistic or superdiffusive transport at intermediate and large lag times [9,10], and also diffusive transport similar to the thermal motion but much faster [11]. Transitions from subdiffusion at $t \lesssim 0.1$ s to superdiffusion at larger t triggered by the action of molecular motors have been observed in several systems [9,10,12–14].

Although there is a vast literature concerning the mathematical modeling of transport by molecular motors in pure viscous environments (see [15–17] and references therein), the modeling of organelle transport in viscoelastic media taking into account the action of individual motors is on its beginnings. In Ref. [18], the authors studied the influence of a viscoelastic fluid on the transport by kinesin with special focus on the calculus of the force-velocity relations and on the analysis of the transient processes. For this, they consider a deterministic version of the generalized Langevin equation (GLE) [19–24] for the motion of the cargo and a detailed stochastic dynamics for the kinesin stepping which takes into account the motion of the two heads. The coupling between the cargo and the motor heads is nonlinear and elastic. In a recent paper [25], the coexistence of normal and anomalous transport by molecular motors inside cells and the delivery efficiency are theoretically analyzed. The authors consider a generalized Kubo-Langevin equation for the organelle position under the influence of a ratchet potential that models the action of a motor. Meanwhile, in a quite recent work [26], the same authors considered

*bouzat@cab.cnea.gov.ar

separate descriptions for motor and cargo to analyze how the power stroke of the motor can beat subdiffusion. These works have interesting precedents on the subject of subdiffusive ratchets [27,28] and dynamics in viscoelastic media [23,24]. In [12], a model based on the GLE was used to interpret a transition from subdiffusion to superdiffusion induced by myosin motors. In that paper, the action of the molecular motors is modeled simply as an external time-correlated noise. Note that all the works just mentioned consider versions of the GLE. This is because in the same way that the standard Langevin equation results in an outstanding model for diffusion of free particles in purely viscous media, the GLE provides a suitable framework for describing subdiffusive motion in viscoelastic media. For this, it includes a friction kernel that weights the history of the velocity and a time-correlated thermal noise related to the kernel through a fluctuation-dissipation relation (see Refs. [20,24] and this work following).

Here, in order to investigate the influence of molecular motors on the motion of particles inside cells, we study the dynamics of an organelle pulled along a linear filament by two opposing motor types in a viscoelastic medium. This can correspond, for instance, to transport by kinesin and dynein on a microtubule [2,17,29,30] or to transport by myosin V and myosin VI along an actin filament [3,4]. We consider the motion of the organelle or cargo as given by a GLE coupled to a stochastic stepping dynamics for the motors. As in the models used in Refs. [17,30–34] for analyzing cargo transport by multiple motors in purely viscous media, the stepping dynamics for the motors is discrete and considers independent elastic linkers for individual motors. It also includes detachment of motors from the filament and attachment of detached motors. The stepping, detachment, and attachment events are ruled by a Monte Carlo type dynamics with probabilities that depend on the force between each motor and the cargo [30,31,33].

In the absence of motors, the GLE model here considered represents a viscoelastic medium with complex modulus $G(\omega) \sim \omega^{\alpha}$ with $0 < \alpha < 1$, in which thermal fluctuations produce a subdiffusive motion of particles characterized by a t^{α} scaling of the MSD. The main purpose of this work is to investigate in which way the action of the molecular motors modifies this behavior at the different scales of the lag time within the range 10^{-5}–10 s which is usually considered in experiments [9,35,36]. We focus on the emergence of superdiffusion at large lag times and on the modification of the subdiffusive properties at small lag times. We discuss our results in connection with important experiments in the literature. In particular, we provide approximate descriptions for results for transport in frog melanocytes [12] and we present a new analysis of the small lag time regime of those experiments. Finally, we study the dynamics under the influence of an external harmonic potential that models the action of an optical trap, and we discuss the effects associated to the dimensionality of the system.

II. MODEL FOR THE MOTION OF A CARGO PULLED BY MOLECULAR MOTORS IN A VISCOELASTIC MEDIUM

A. Cargo motion

As stated in the Introduction, we are interested in analyzing the mean square displacement (MSD) of particles transported along a linear filament by molecular motors. Our modeling framework will thus be mainly one dimensional, although at the end of this work we discuss the case of bidimensional motion.

Our starting point for modeling is the one-dimensional generalized Langevin equation (GLE) [20–22,24] which describes the subdiffusive motion of a particle in a viscoelastic medium in close to equilibrium [20] conditions

$$m\ddot{x}(t) = -\int_0^t \gamma(t-t')\dot{x}(t')dt' + \xi(t). \tag{1}$$

Here, $x(t)$ is the position of the particle, m is its mass, $\gamma(t)$ is the frictional kernel given by

$$\gamma(t) = \frac{\gamma_0}{\Gamma(1-\alpha)} t^{-\alpha}, \tag{2}$$

and $\xi(t)$ is the time-correlated Gaussian thermal noise satisfying the fluctuation-dissipation relation

$$\langle \xi(t)\xi(t') \rangle = k_B T \gamma(t-t'). \tag{3}$$

The parameters α $(0 < \alpha < 1)$ and γ_0 $(\gamma_0 > 0)$ characterize the properties of the viscoelastic medium in a way that we later indicate in connection with the viscous modulus. Equation (1) produces subdiffusive motion with logarithmic slope α [20,23,24]. The diffusive limit in which the MSD has logarithmic slope $\alpha = 1$ is described by the standard Langevin equation with friction term $-\gamma_0 \dot{x}(t)$ and white Gaussian thermal noise. This corresponds to a pure viscous medium. For a detailed explanation of this limit in connection with Eq. (1), see [24].

Equation (1) with the same kernel and noise was studied in many works (see [12,19–24,35–37] and references therein) since it constitutes an outstanding model for subdiffusive motion in viscoelastic media. The particular functional form of the kernel is found to be the only one that produces subdiffusion given the fluctuation-dissipation relation (3) and three additional conditions on $\xi(t)$ which are important on physical grounds [20]. Namely, that the associated generalized Wiener process $B(t)$ [i.e., the stochastic process such that $\xi(t) = dB(t)/dt$] should be Gaussian, self-similar, and with stationary increments [20]. The process $B(t)$ is called *fractional Brownian motion*, while its derivative $\xi(t)$ is known as the *fractional Gaussian noise* [20]. The model has also a clear microscopic interpretation since it can be derived [20,24] by assuming that the particle interacts harmonically with a large number of *environmental* particles which are in turn able to move due to these interactions. The right hand side of Eq. (1) emerges as the continuous limit of the sum of the forces exerted by the environmental particles [20,24]. Note that in [20] and other works, the theory is developed using the Hurst parameter $H = 1 - \alpha/2$ instead of α.

Now, we introduce our model for the motion of an organelle (or cargo) driven by molecular motors along an actin filament or microtubule in a viscoelastic medium. We consider the dynamics of the organelle as given by the overdamped limit of Eq. (1) with the addition of a harmonic force $-ax(t)$ representing the action of an optical trap, plus another force term $F_M(x(t),t)$ which stands for the action of the molecular

motors. We get

$$\int_0^t \gamma(t-t')\dot{x}(t')dt' = -ax(t) + F_M(x(t),t) + \xi(t), \quad (4)$$

with $\gamma(t)$ and $\xi(t)$ defined as before. Note that the parameter a is just the elastic constant associated to the harmonic potential representing the optical trap. The force $F_M(x(t),t)$ will be determined by the stochastic stepping dynamics for the molecular motors that we introduced later.

The overdamped limit is considered because the motion of particles inside cells shows inertial effects only for lag times of the order 10^{-6} s or lower [35,36], while here we analyze the range from 10^{-5}–10 s. As we later show, the consideration of the overdamped limit gives us relevant computational advantages for the numerical treatment of the system. It is important to mention that the formal procedure of setting $m = 0$ in Eq. (1) to obtain the overdamped equation is mathematically well defined. This is indicated for instance in [20], where the author studies the overdamped Eq. (4) with $F_M(x(t),t) = 0$ considering the pathway interpretation to find the covariance of $x(t)$ for the general case $a \neq 0$. Moreover, it is also shown in the developments in [35], where the authors study the solutions for the MSD in the overdamped limit.

Before introducing the Monte Carlo stepping dynamics describing the motion of the molecular motors, we provide a Markovian approximation for Eq. (4) that enables for an easy numerical solution of the system. Note that the numerical treatment is unavoidable since the forces $F_M(x(t),t)$ will be determined by the motor's dynamics.

B. Markovian approximation and numerical solution for the overdamped generalized Langevin equation

Here, we search for a Markovian approximation to Eq. (4). At this instance, $F_M(x(t),t)$ can be considered as an arbitrary function. Our approach is based on the one given in [23] for solving the underdamped equation

$$m\ddot{x}(t) = F_M(x(t),t) - \int_0^t \gamma(t-t')\dot{x}(t')dt' + \xi(t), \quad (5)$$

with $\gamma(t)$ and $\xi(t)$ as in Eqs. (2) and (3). The method in [23] (see also [24] for a review) uses the fact that the noise $\xi(t)$ can be approximated by a sum of independent Ornstein-Uhlenbeck noise components, while the power law of the memory kernel can be approximated by a sum of exponentials as

$$\gamma(t) \simeq \sum_{i=0}^{N-1} \eta_i \exp(-\nu_i t). \quad (6)$$

Here, the constants η_i and ν_i, $i = 0, \ldots N-1$ are defined in terms of a high-frequency cutoff for the noise called ν_0, and a scale parameter b as $\eta_i = [\gamma_0/\Gamma(1-\alpha)]C_\alpha(b)\nu_0^\alpha/b^{i\alpha}$ and $\nu_i = \nu_0/b^i$. Finally, $C_\alpha(b)$ is a constant that can be chosen in such a way that Eq. (6) results in a good approximation for $1/\nu_0 < t < b^{(N-1)}/\nu_0$ [23].

With these definitions, Ref. [23] shows that the non-Markovian dynamics of Eq. (5) can be well approximated by the Markovian system

$$\begin{aligned} m\ddot{x}(t) &= F_M(x(t),t) + \sum_{i=0}^{N-1} u_i(t), \\ \dot{u}_i(t) &= -\eta_i\dot{x}(t) - \nu_i u_i(t) + \sqrt{2\nu_i\eta_i k_B T}\zeta_i(t), \end{aligned} \quad (7)$$

which is called a *Markovian embedding* [23] for Eq. (5). Here, $u_i(t)$ with $i = 0, \ldots N-1$ are N auxiliary variables, while $\zeta_i(t)$ are white Gaussian noises satisfying $\langle\zeta_i(t)\zeta_j(t')\rangle = \delta_{ij}\delta(t-t')$. The initial values $u_i(0)$ have to be sampled from unbiased Gaussian distributions with standard deviations $\sigma_i = \sqrt{k_B T\eta_i}$. The fact that the dynamics behind Eq. (7) is Markovian becomes clear by noting that it is possible to redefine the system in terms of variables $p(t) \equiv m\dot{x}(t)$, $x(t)$, and $u_i(t)$ using only first order stochastic differential equations.

Note that, according to Eqs. (5) and (7), given the variables $u_i(t)$ satisfying the second Eq. (7), within the framework of the Markovian approximation we have the formal equivalence

$$-\int_0^t \gamma(t-t')\dot{x}(t')dt' + \xi(t) = \sum_{i=0}^{N-1} u_i(t). \quad (8)$$

Let us now go back to the overdamped system of Eq. (4). By replacing the power-law kernel by the approximation (6) so that we get a finite value $\gamma(t=0)$, we can perform an integration by parts of the left hand side of Eq. (4). Then, assuming $x(t=0) = 0$ for the sake of simplicity, we get

$$\begin{aligned} &\gamma(0)x(t) + \int_0^t \gamma'(t-t')x(t')dt' \\ &\quad = -ax(t) + F_M(x(t),t) + \xi(t), \end{aligned} \quad (9)$$

where $\gamma'(t) = \sum_{i=0}^{N-1}(-\nu_i\eta_i)\exp(-\nu_i t)$. This is just

$$\begin{aligned} &\left(a + \sum_{i=0}^{N-1}\eta_i\right)x(t) \\ &\quad = F_M(x(t),t) - \int_0^t \gamma'(t-t')x(t')dt' + \xi(t). \end{aligned} \quad (10)$$

Now, using the formal relation of Eq. (8) with $\gamma'(t-t')$ instead of $\gamma(t-t')$ and $x(t)$ instead of $\dot{x}(t)$, we get to the following Markovian approximation for the non-Markovian equation (4):

$$\begin{aligned} x(t) &= \frac{1}{a + \sum_{i=0}^{N-1}\eta_i}\left(F_M(x(t),t) + \sum_{i=0}^{N-1} u_i(t)\right), \\ \dot{u}_i(t) &= \nu_i\eta_i x(t) - \nu_i u_i(t) + \sqrt{2\nu_i\eta_i k_B T}\zeta_i(t), \end{aligned} \quad (11)$$

where $\eta_i, \nu_i, \zeta_i(t)$ and $u_i(0)$ are defined as before. Note that the term $-\eta_i\dot{x}(t)$ on the right hand side of Eq. (7) has changed to $\nu_i\eta_i x(t)$ in Eq. (11).

It is interesting to note that only the evolution of the N variables $u_i(t)$ is nontrivial since $x(t)$ is formally determined at each time by the sum $\sum_i u_i(t)$. In particular, for the case of the stochastic dynamics for motors that we later introduce, the dependence of $F_M(x(t),t)$ on $x(t)$ is piecewise linear. This enables the integration of Eqs. (11) using Euler or Runge-Kutta stochastic methods [38] which are explained in the Supplemental Material [39]. Time steps in the range

5×10^{-8} s $\leqslant dt \leqslant 5 \times 10^{-6}$ s are used depending on the values of γ_0 and α and on the value chosen for ν_0. We found that the larger the ν_0, the smaller the value of dt needed to obtain algorithm stability and the better the approximation to the analytical solution for the MSD that we describe below. In most of our calculations, we consider a number $N = 16$ of modes $u_i(t)$ with the scale parameter $b_0 = 5$, and $\nu_0 = 5 \times 10^{-7}$. The constant $C_\alpha(b)$ is always of order 1 and chosen as the one that minimizes the square distance associated to the approximation (6). For instance, we get $C_{3/4}(5) = 1.3124$ and $C_{1/2}(5) = 0.91$ for $\nu_0 = 5 \times 10^{-7}$. Embeddings with $N = 32$ and different values of b, ν_0, and dt were used in order to check the results of some selected examples.

Importantly, in Refs. [24–28], the authors studied a more general overdamped GLE which, compared to Eq. (4), includes an additional friction term $\mu\dot{x}$ and its corresponding white noise with correlation proportional to $\mu\delta(t - t')$. It can be shown that the Markovian embedding given in Eqs. (11) can also be obtained as the $\mu \to 0$ limit of the embedding considered in [24–28] for this system. In the Supplemental Material [39], we study in some detail the relation between the two overdamped Markovian dynamics and show that they give essentially the same results provided a small enough value of μ is considered.

C. Dynamics without molecular motors: Testing the Markovian approximation

Here, we check the validity of the Markovian approximation by comparing the numerical solution of Eqs. (11) with analytical results known for Eq. (4) for the case $F_M(x(t),t) = 0$, and with numerical results for the underdamped system (7).

The main quantity we are interested in is the mean square displacement (MSD) of the particles in the viscoelastic medium as a function of the lag time. For a single trajectory $x(t)$ sampled at times $t_i = i\delta t$ with $i = 0,1,2,\ldots,N$ after skipping an initial nonstationary stage, the MSD as a function of the (discrete) lag time $t \ll N\delta t$ is computed as

$$\Delta x(t)^2 = \frac{1}{N - t/\delta t} \sum_{i=1}^{N-t/\delta t} [x(i\delta t + t) - x(i\delta t)]^2. \quad (12)$$

Then, we average over realizations to get the ensemble averaged mean square displacement $\rho(t) = \langle \Delta x(t)^2 \rangle$. For the sake of simplicity we refer to $\rho(t)$ as the MSD. Throughout this work, we consider $\delta t = 10^{-5}$ s.

The analytical results for the MSD of particles with overdamped dynamics given by Eq. (4) with $F_M(x(t),t) = 0$ and $a = 0$ is known to be [35]

$$\rho(t) = \frac{2k_BT}{\gamma_0\Gamma(1+\alpha)} t^\alpha. \quad (13)$$

Meanwhile, for $a \neq 0$ (i.e., in the presence of a harmonic potential) the MSD is given by [35]

$$\rho(t) = \frac{2k_BT}{a}\left[1 - E_\alpha\left(-\frac{a}{\gamma_0}t^\alpha\right)\right]. \quad (14)$$

Here, $E_\alpha(y)$ is the Mittag-Leffler function (see [20,22] and further references therein). It is important to stress that this analytical result is valid only if the time averages of Eq. (12) are performed on the stationary stages of the trajectories. Moreover, it is worth noting that the direct ensemble averaging of the displacements (without temporal average first) yields a different result [40].

Let us first consider the case $a = 0$. Figure 1(a) compares the MSD results from simulations of Eqs. (11) with the analytical result given in Eq. (13) considering the parameters $\alpha = 0.75$ and $\gamma_0 = 7.2 \times 10^{-4}$ pN s$^\alpha$/nm, which are compatible with those measured in cultured human cells [35]. The very good agreement between the numerical solution for the Markovian approximation and the exact solution for the system (4) is apparent. Only for $t \lesssim 5 \times 10^{-4}$ s the approximation slightly overestimates the analytic result (the logarithmic slope is slightly underestimated). This error can be decreased by simultaneously increasing ν_0 and decreasing dt but with a considerable growth of the computational cost. Figure 1(a) also shows MSD results for the underdamped system (7) considering the same values of α and γ_0 and a mass $m = 2 \times 10^{-7}$ g. We see that for the underdamped system, the behavior $\rho(t) \sim t^\alpha$ matching the ovedamped dynamics is found only for lag times larger than the crossover time $\tau_p = (m/\gamma_0)^{1/(2-\alpha)} = 0.0014$ s [23,35]. For smaller lag times, the MSD of the underdamped system is ballistic ($\sim t^2$)

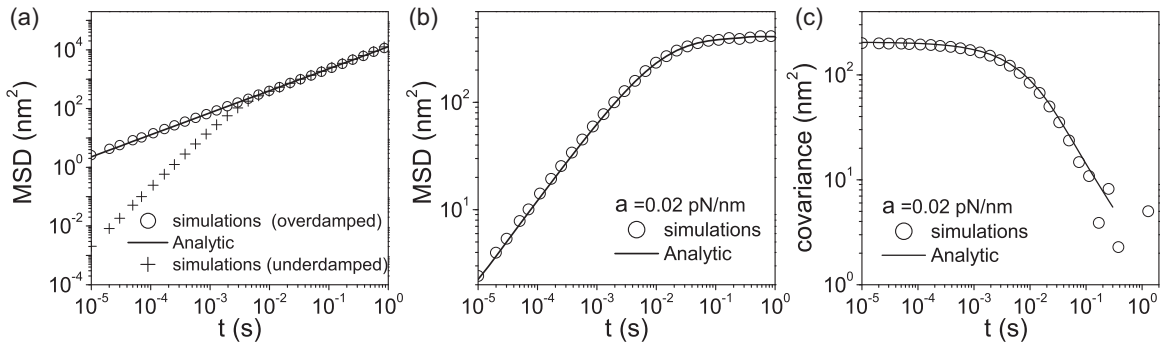

FIG. 1. Dynamics without molecular motors [$F_M(x(t),t) = 0$]. (a) MSD results for $a = 0$. The circles indicate simulations from the Markovian approximation (11) for Eq. (4) with $\nu_0 = 5 \times 10^{-7}$/s and $dt = 5 \times 10^{-8}$ s, the solid line corresponds to the exact analytical solution in Eq. (13), and the crosses correspond to the underdamped dynamics with $m = 2 \times 10^{-7}$ g. (b) MSD results for $a = 0.02$ pN/nm. The circles correspond to the numerical solution of Eqs. (11), while the solid line corresponds to the analytic result in Eq. (14). (c) Results for the covariance for the same system studied in (b), comparison between analytic (solid line) and numerical solution (circles). In all the cases, the parameters considered are $\alpha = 0.75$ and $\gamma_0 = 7.2 \times 10^{-4}$ pN s$^\alpha$/nm.

as expected [23,36]. Note that the value of the mass here considered is about 10^6 times larger than the actual masses of the organelles in cellular systems, which are typically of the order $m \sim 10^{-13}$ g [35] (considering water density and radius of the order of half-micron). Realistic masses lead to much smaller crossover times of order $\tau_p \lesssim 10^{-6}$ s or lower, as those recently found in [36]. The numerical solution of Eqs. (7) with realistic values of the mass would demand a time discretization with steps of the order 10^{-12} s or lower. This means much smaller than those used here. This clearly shows the relevance of the consideration of the overdamped dynamics for analyzing the region of lag times $t > 10^{-6}$ s, where the MSD behavior is expected to be nonballistic [5,36].

Now, we analyze the case $a \neq 0$. First, Fig. 1(b) shows that the numerical solution of Eqs. (11) correctly matches the analytical result for $\rho(t)$ given in Eq. (14). The value considered for the elastic constant of the harmonic potential is $a = 0.02$ pN/nm, which is in the range of those recently used in experiments in optical trapping microrheology [35]. Finally, in Fig. 1(c) we compare the results for the covariance $\langle x(t_0)x(t_0+t)\rangle$ (where $\langle \ldots \rangle$ indicate average both on the initial time t_0 and ensemble) computed from the numerical solution of Eqs. (11), with the expected analytic result given in [20]

$$\langle x(t_0)x(t_0+t)\rangle = \frac{k_B T}{a}\left[E_\alpha\left(-\frac{a}{\gamma_0}t^\alpha\right)\right]. \tag{15}$$

Again, the numerical approximation correctly matches the exact theory. It is worth mentioning that for $t \gtrsim 0.2$ s our algorithm for computing the Mittag-Leffler function loses stability when calculating the analytic covariance, while the statistics of the simulations becomes poor.

D. Relation between the overdamped GLE and the complex modulus

The rheological properties of an isotropic viscoelastic medium are characterized by the complex modulus $G(\omega)$ [5] of the material which quantifies the stress response of the medium to an applied oscillatory deformation of frequency ω. The real part of the complex modulus is the elastic modulus $G'(\omega)$ which measures the *in-phase* response to the deformation [5], while the imaginary part $G''(\omega)$ is the viscous modulus that characterizes the *out-of-phase* response. A purely viscous material (with very small elasticity, like water) has $G'(\omega) \simeq 0$, while a purely elastic material (like a solid rubber) has $G''(\omega) \simeq 0$. In general, the cell cytoplasms have nonvanishing $G'(\omega)$ and $G''(\omega)$ and are thus viscoelastic. The viscoelastic properties of the cells are usually measured taking into account the relation between the complex modulus and the MSD of particles embedded in the medium. In fact, the amplitude of the complex modulus can be well approximated as [5,7,18,35]

$$|G(\omega)| = \left.\frac{k_B T}{\pi R\langle \Delta r(t)^2\rangle \Gamma[1+\alpha(t)]}\right|_{t=1/\omega}, \tag{16}$$

where R is the radius of the particle, $\langle \Delta r(t)^2\rangle$ is the mean square displacement measured in three dimensions, and $\alpha(t)$ is the local logarithmic slope of $\langle \Delta r(t)^2\rangle$. Meanwhile, the elastic and viscous modulus are given by $G'(\omega) = |G(\omega)|\cos[\pi\alpha(1/\omega)/2]$ and $G''(\omega) = |G(\omega)|\sin[\pi\alpha(1/\omega)/2]$, respectively [5,7,35].

Within the model of Eq. (4), in the absence of molecular motors and considering $a = 0$, we have that $\langle \Delta r(t)^2\rangle$ is just three times the value of $\rho(t)$ given in Eq. (13), while $\alpha(t)$ coincides with the constant value α. Thus, Eq. (4) with $a = 0$ and $F_M(x(t),t) = 0$ represents a viscoelastic medium with

$$|G(\omega)| = \frac{\gamma_0 \omega^\alpha}{6\pi R}. \tag{17}$$

As mentioned before, the extreme case $\alpha = 1$ represents a purely viscous medium with $G'(\omega) = 0$ while for $\alpha = 0$ we obtain a purely elastic medium with $G''(\omega) = 0$. Note that the parameter γ_0 has units that depend on α and so the way in which it characterizes the properties of the system is rather unintuitive. For instance, it is meaningless to compare systems with a constant numerical value of γ_0 and different values of α. Therefore, following [18] we consider a different dimensionless parameter to describe the properties of the medium instead of γ_0. Namely, the ratio n_w of the viscous modulus of the medium to that of water, both measured at a low reference frequency [18]. We define [18] $n_w = G''(\omega_r)/G''_w(\omega_r)$ with $G''_w(\omega) = \eta_0\omega$ the viscous modulus of water, η_0 the viscosity of water, and considering the low reference frequency $\omega_r = 2\pi/(100s)$. With this definition we get

$$\gamma_0 = \frac{6\pi R\eta_0 \omega_r^{1-\alpha}}{\sin(\pi\alpha/2)} n_w, \tag{18}$$

which is the value we consider in Eq. (4) given the desired values of α, n_w, and R. Note that in the case of a purely viscous fluid (i.e., $\alpha = 1$), Eq. (18) leads to the standard Stokes formula $\gamma_0 = 6\pi R\eta$, with $\eta = n_w\eta_0$, which is used in most works on cargo transport in viscous media [17,30–33].

E. Molecular motors stochastic dynamics

Here, we introduce the model for the molecular motors stochastic dynamics that we use to define the force $F_M(x(t),t)$ in Eq. (4). As indicated in the Introduction, we consider a discrete stepping dynamics based on the models analyzed in [17,30,31,33,34]. From the point of view of modeling, the main newness in this work is the combination of the stepping dynamics for motors with the GLE for the cargo motion since all the mentioned previous works considered either nonviscosity or a purely viscous medium.

The model considers that each molecular motor constitutes an elastic linker between the organelle and the filament. This linker moves in discrete steps on the filament transporting the cargo in a preferred direction [17,30–34]. This mechanical picture is common to microtubule-based [16,17,30,31,33] and actin-based [4] transport, although it has been much more extensively studied for microtubule transport.

Usually, the transport of a single organelle is mediated by several motors [2,4,15,30,32]. In the case that both plus-end and minus-end motors participate of the transport (for instance, kinesin and dynein on microtubule transport [2,15,30] or myosin V and myosin VI on actin [4]) the transport is *bidirectional*. This means that the organelle can move back and forth on the filament [4,15,17,30]. The way in which the bidirectional transport is coordinated and regulated is today a subject of very active research [4,15–17,29] and may differ from one system to another, but it is clear that the motors

can detach from the filament and also rebind after some time. Thus, the direction of the motion is determined essentially by the species that dominates at each time. When both motor types are pulling the cargo at the same time, the motion of the organelle is temporally paused (or the velocity considerably reduced). This is called the *tug of war* effect [4,15,30].

We consider the force $F_M(x(t),t)$ in Eq. (4) [and in its Eq. (11)] as due to the action of two types of motors with opposite polarities that move along the same x coordinate used to represent the cargo position on the filament. The organelle is assumed to be linked permanently to N_f forward motors (which advance in the positive direction) and N_b backward motors (which advance in the negative direction). At a given time, each motor may be either engaged on the filament or detached. The allowed positions for engagement of motors are the discrete sites $x_j = j\Delta x$ with integer j. Values $\Delta x = 8$ or 32 nm are considered in agreement with the experimental findings for different motor types [41,42].

As in Refs. [17,18,30–33], each engaged motor is considered as a nonlinear elastic linker that can only exert an attractive force provided a critical distance x_0 (i.e., the maximum relaxed length of the linker) is surpassed. Let $x_i(t)$ be the position of engagement of the motor i (that we refer to as the position of the motor i) and $x(t)$ the position of the cargo. The force $f_i(t)$ exerted by the motor i on the cargo is defined as follows [17,18,30–33]. For $x_i(t) > x(t) + x_0$, we set $f_i(t) = k_i[x_i(t) - (x(t) + x_0)]$, where $k_i > 0$ is the stiffness of the motor i. Note that in this case we have $f_i(t) > 0$ and, thus, the motor pulls to the positive direction (i.e., to the right). Meanwhile, for $x_i(t) < x(t) - x_0$, we set $f_i(t) = k_i[x_i - (x(t) - x_0)]$. Hence, we have $f_i(t) < 0$ and thus the motor pulls to the left. Finally, for motors engaged at positions satisfying $|x(t) - x_i(t)| \leqslant x_0$ as well as for detached motors, we set $f_i(t) = 0$. It is important to stress that, normally, forward motors pull to the right while backward motors pull to the left. However, due to fluctuations in the cargo position, a forward (backward) motor can pull to the left (right) for a short time interval [32] (see Fig. 1 in the Supplemental Material [39] for a description of the different motor-cargo configurations).

Now, we call $\mathcal{R}(t)$ the set of motors that pull to the right at time t, $\mathcal{L}(t)$ the set of motors that pull to the left, and $\mathcal{P}(t) = \mathcal{R}(t) \cup \mathcal{L}(t)$ the set of all the *pulling* motors [32]. Then, the force $F_M(x(t),t)$ defined as the sum of the nonvanishing forces $f_i(t)$ can be written as

$$F_M(x(t),t) = -\left(\sum_{\mathcal{P}(t)} k_i\right) x(t) + \left(\sum_{\mathcal{P}(t)} k_i x_i(t)\right) - \left(\sum_{\mathcal{R}(t)} k_i\right) x_0 + \left(\sum_{\mathcal{L}(t)} k_i\right) x_0, \qquad (19)$$

where $\sum_{\mathcal{P}(t)}$, $\sum_{\mathcal{R}(t)}$, and $\sum_{\mathcal{L}(t)}$ indicate sum over the motors belonging to $\mathcal{P}(t)$, $\mathcal{R}(t)$, and $\mathcal{L}(t)$, respectively.

The motion of the motors is determined by the forces $-f_i(t)$ exerted by the organelle on the motors. In order to get expressions for the stepping probabilities valid both for forward and backward motors, the motor's dynamics will be given in terms of the load forces $L_i(t)$, which are defined as $L_i(t) = f_i(t)$ for forward motors and $L_i(t) = -f_i(t)$ for backward motors. With these definitions, $L_i(t)$ is positive if the force that the cargo exerts on the motor i acts against the polarity of the motor, while $L_i(t) < 0$ indicates an assisting force. For simplicity, from now on we do not indicate the time dependence of the load forces $L_i(t)$ and just write L_i.

We consider that each engaged motor performs a step of length Δx toward its polarity with a probability per time unit equal to $p_{\text{step}}(L_i) = v(L_i)\Delta x$. Here, $v(L_i)$ is the mean velocity of the motor as a function of the load force. This function is usually measured in experiments using optical traps [17,42]. In agreement with experimental results for different motor types [15,31,42], we consider $v(L_i) = v_0[1 - (L_i/F_s)^w]$ for $0 \leqslant L_i < F_s$, with F_s the stall force and w the exponent of nonlinearity [31]. Meanwhile, we set $v(L_i) = 0$ for $L_i \geqslant F_s$ and $v(L_i) = v_0$ for $L_i < 0$ (assisting forces) [31,32,42]. It is important to stress that, although the parameter v_0 is considered positive both for forward and backward motors in order to obtain positive stepping rates, forward motors always step toward the positive direction (i.e., to the right) while backward motors always step to the left.

The detachment rates of the motors are usually assumed to grow exponentially with the load force [15,31], following the results found in pioneering experiments [42] and the theoretical concepts of the Kramers theory. However, recently [17] it has become clear that, at load forces of the order of the stall and larger, the detachment rates for different motors show a saturation effect or even a decrease with the load. Here, we take into account this fact considering an exponential growth at small forces and saturation at large forces. We consider that each motor detaches from the filament with a probability per time unit given by $\epsilon \exp[|L_i|/F_d]$ for $|L_i| \leqslant F_s$ and $\epsilon \exp[F_s/F_d]$ for $|L_i| > F_s$, where ϵ is the zero-load detachment rate and F_d is the detachment force of the motor [15,17,31].

Finally, following the assumptions in [15,17,30,31,33], we consider that a detached motor reattaches to the filament with constant probability per time unit Π. The engagement occurs with equal probability in any of the discrete sites x_j satisfying $|x_j - x(t)| < x_0$ [32,33]. This means that it is assumed to occur with the nonlinear spring relaxed. In general, the set of parameters v_0, F_s, F_d, ϵ, Π, x_0, and Δx, as well as the stiffnesses of the motors, can be different for forward and backward motors. However, as we later explain, in this paper we focus mainly on the symmetric situation in which both motor species have the same parameters.

A detailed description of the computational procedure for evolving the motor dynamics can be found in [39]. The complete model of cargo plus motors thus couples the Eq. (4) and the motor dynamics through the forces f_i. This is done in the same way as in models in [17,30–33] but considering the overdamped GLE instead of the standard Langevin equation [32,33] or other purely viscous dynamics [17,30,31].

III. ORGANELLES DRIVEN BY MOLECULAR MOTORS IN VISCOELASTIC MEDIA

A. Simulations and system parameters

In several systems showing bidirectional transport by two opposing motor species [17,29,43], the parameters of both motor types are found to be similar to each other, and the

transport is approximately symmetric. Hence, we focus our analysis on the motion of organelles pulled along a filament by two opposing motor teams of equal number of motors and parameters. The symmetry assumption is not rigorous for transport by myosin V and myosin VI since myosin V is dominant 79% of the time [4]. However, as we will show when analyzing the transport by a single motor species in connection with a particular experiment, our main results and conclusions are independent of the symmetry assumption.

Using Eqs. (11) coupled to the stochastic stepping dynamics for motors we generate trajectories of 25 s long. In the case that all the motors are detached before the maximal time, the simulation is not interrupted and the motors are allowed to engage again. Then, considering Eq. (12) with $\delta t = 10^{-5}$ s and averaging over runs we compute the ensemble averaged MSD for the range of lag times 10^{-5} s $< t <$ 10 s. In most cases, the average is done over 100 realizations. For some special examples in which lag times larger than 10 s result relevant, trajectories of 50 or 100 s long are considered.

As we are interested in analyzing phenomena that may occur in different systems, we vary the system parameters over relatively wide ranges. This enables us to identify the effects of each parameter on the dynamics and to check the robustness of our main results. For our scanning of the parameter space we consider a reference parameter set (RS) and then we change each parameter over a reasonable range. The parameters of the RS are the following. We consider $\alpha = 0.75$, which is the value found in cell systems at low lag times [5,9,35] and explained in base of the theory of semiflexible polymers [8]. An organelle radius $R = 400$ nm, the standard room temperature $k_BT = 4.1$ pN nm, and a ratio between viscosity and water viscosity at low frequencies $n_w = 176$. Using the water viscosity $\eta_0 = 10^{-9}$ pN s/(nm)^2, this leads to $\gamma_0 = 7.2 \times 10^{-4}$ pN s$^{3/4}$/nm, which is the value used in Fig. 1 and recently found in human cells in [35]. Meanwhile, the parameters considered in the RS for the stochastic dynamics of motors are $N_f = N_b = 1$, $k = 0.3$ pN/nm, $\Delta x = 8$ nm, $x_0 = 100$ nm, $v_0 = 500$ nm/s, $w = 2$, $F_s = 2.5$ pN, $\epsilon = 0.25$/s, $F_d = 3$ pN, and $\Pi = 1$/s. Note that $k = 0.3$ pN/nm is the value measured for kinesin and also considered usually for dynein in stochastic models [17,30,33]. $\Delta x = 8$ nm is the step length measured for kinesin while $x_0 = 100$ nm is a typical length for different motors [1]. When varying the parameters we consider also $\Delta x = 32$ nm [41], and $x_0 = 70$ nm, with no relevant changes in our results. The velocity $v_0 = 500$ nm/s is a standard value for molecular motors [1,4,17]. Stall forces $F_s \simeq 2.5$ pN were recently found *in vivo* both for kinesin and dynein [17,29] and are also in the range of those found for myosin [4]. More standard values for kinesin and dynein of order 5 pN are also analyzed when varying the parameters.

In Fig. 2, we show four typical trajectories for an organelle generated with the parameters of the RS. As expected, bidirectional motion with plus and minus runs is observed. Reversion of the motion can occur with or without intermediate pauses [15].

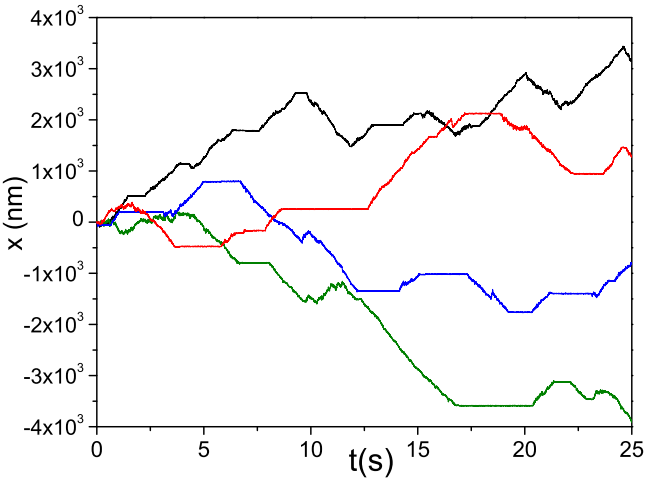

FIG. 2. (Color online) Trajectories for organelles pulled by molecular motors. Simulations of Eqs. (11) with $a = 0$ and $F_M(x(t),t)$ given by the stochastic dynamics for motors. In all the cases, the parameters are those of the RS.

B. Results for the mean square displacement

In Fig. 3, we show the MSD results for the RS considering the dynamics of the Eqs. (11) with motors (i.e., coupled to the stochastic dynamics of motors) and without motors [i.e., setting $F_M(x(t),t) = 0$]. The molecular motors modify the $\rho(t) \sim t^\alpha$ behavior of the viscoelastic medium in various ways at different ranges of the lag time. In fact, we can identify four different regimes for the MSD of the system with motors, that in the figure are separated by the displayed times $t_1 = 5 \times 10^{-5}$ s, $t_2 = 0.016$ s, and $t_3 = 3$ s. First, for very short lag times ($t < t_1$), the MSD tends to the t^α behavior of the system without motors. Then, for $t_1 < t < t_2$, we find a subdiffusive regime with a well defined value of the logarithmic slope of $\rho(t)$ smaller than α, which for the RS is approximately 0.57. Then, at t_2, a relatively slow crossover to a superdiffusive regime starts. The superdiffusive regime is well established at lag times of order 0.1 s $\simeq 5 \times t_2$ with a power-law behavior

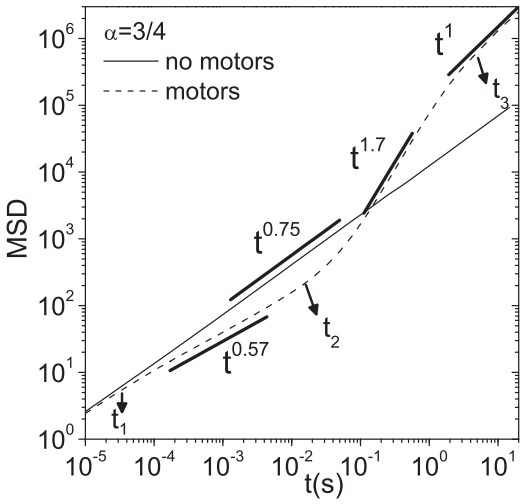

FIG. 3. MSD vs lag time for the RS with $a = 0$. The solid line corresponds to $F_M(x(t),t) = 0$ while the dashed line corresponds to the results with $F_M(x(t),t)$ given by the stochastic dynamics for motors with the RS. The times t_1, t_2, and t_3 indicate the changes of regimes (see text). The solid segments indicate different power-law behaviors found.

$\rho(t) \sim t^{1.7}$ for the RS. Finally, at lag times larger than $t_3 \sim 3$ s, we find a pure diffusive regime with $\rho(t) \sim t$.

The four regimes of $\rho(t)$ can be understood by analyzing the role played by the motors on the determination of the cargo dynamics at the different time scales. First, the crossover from subdiffusion to superdiffusion occurs at a region of lag times at which the steps of the motors begin to be appreciable. In fact, we have defined t_2 as the mean time between two steps of an unloaded motor, which is just $\Delta x/v_0 = 0.016$ s for the RS. Clearly, during a time interval larger than a few times t_2 (i.e., $t \sim 0.1$ s) we may observe several motor steps and, thus, processive motion leading to superdiffusion. In contrast, during time intervals much smaller than t_2, the motors are essentially stalled and act as static crosslinkers which contribute to reduce the mobility of the cargo. This leads to the subdiffusive regime with a logarithmic slope smaller than α observed at $t < t_2$. As we later explain, this reduction of the slope of the MSD at short lag times due to the action of motors is observed in the results of the experiments for myosin V driven transport in frog melanocytes presented in [12].

The time t_3 of the order of a few seconds which characterizes the transition from superdiffusive motion to diffusive motion is the typical time between reversions from plus to minus processive motion (see Fig. 2). Thus, the diffusive motion at lag times $t > t_3$ is due to the fact that the cargo comes back and forth in symmetric bidirectional processive motion. Recall that the motion is symmetric due to that the parameters of forward and backward motors are the same. In case that this hypothesis is abandoned, the long time behavior is expected to change, as we later show.

For very short lag times ($t < t_1$), the thermal fluctuations dominate the dynamics. The convergence of the MSD for the system with motors to that of the systems without motors occurs for values of the lag time such that $\rho(t)$ itself is lower than 10 nm^2. This corresponds to position changes in the range of a few nanometers. Although the motors act as static crosslinkers, at such small time and space scales there is no confinement of the cargo by the elastic constants k of the crosslinkers. We can understand this by analyzing the motion of the cargo in a harmonic potential of constant k equal to that of the motor linker. This is exactly the same system as that analyzed in Fig. 1(b), with analytic solution given in Eq. (14), but with elastic constant $k = 0.3$ pN/nm instead of $a = 0.02$ pN/nm. Note that the asymptotic (confinement) value of the MSD for a particle is $2k_BT/k$. Thus, considering the value $k \sim 0.3$ pN/nm for the motor linkers in the RS, we obtain $\sim$27 nm^2 as the confinement value of the MSD by a static motor. Clearly, at lag times $t < t_1$ in Fig. 3 we have $\rho(t) \ll 27$ nm^2, thus, we are still in the $\rho(t) \sim t^\alpha$ regime. These are of course unrefined arguments since our model includes two motors with nonlinear springs so that the confinement conditions depend on the relative positions of the motors and do not correspond to a simple harmonic potential.

In Fig. 4, we analyze the dependence of the MSD on the values of the parameters that regulate the motor's dynamics. We find that in all the cases studied, the qualitative shape of the $\rho(t)$ curve is the same as that shown in Fig. 3. Thus, the results before analyzed are robust to changes of the parameters. Figure 4(a) shows results for $N_f = N_b = 2$ considering two different values of ϵ and compares with the RS case with $N_f = N_b = 1$. We see that the change generated by the increasing of the number of motors can be compensated approximately by a decreasing of the detachment rates. Figure 4(b) analyzes the dependence on v_0. It can be seen that, as v_0 grows, the transition to the superdiffusive regime occurs at smaller values of t following the decreasing of the transition time $t_2 = \Delta x/v_0$ (indicated with vertical segments). Figure 4(c) shows that an increasing of the stall force to a value $F_s = 5$ pN (typical for kinesin and dynein in several systems) produces an upward shift of the MSD curve without changing its form. The dependence on ϵ [Fig. 4(d)] is more involved, as this parameter (in addition to N) is the main one responsible for defining the typical times of plus and minus runs, pauses, and complete detachment of the organelle [33]. In fact, the cargo dynamics has been shown to be particularly sensitive to changes in the value of ϵ for the case of purely viscous media [32]. Figure 4(e) shows that the MSD curves are shifted to the right when the attachment rate Π is increased. Finally, Figs. 4(f), 4(g) and 4(h) show that variations of the parameters k, Δx, and w produce tiny effects on the MSD results. The most remarkable one is the dependence of $\rho(t)$ on k at small lag times, which indicates that the time t_1 at which the effects of the motors begin to be appreciable decreases with k. This could be expected taking into account the argument given above concerning the confinement by a static crosslinker and its relation with t_1.

In Fig. 5, we analyze the dependence of the MSD on the parameters α and n_w characterizing the properties of the viscoelastic medium. Again, we verify the robustness of the results shown in Fig. 3. As could be expected, while α controls the average slope of the $\rho(t)$ curves [Fig. 5(a)], a growth of n_w produces a quasiparallel shift of the curves to smaller values of the MSD [Fig. 5(b)]. In Fig. 5(c), we show the ratio of the MSD values of the two solid curves shown in Fig. 5(b). For $t \to 0$, the ratio converges to that expected for two systems without motors (i.e., the quotient of the two involved n_w values), while for larger values of t the ratio oscillates but remaining below its $t \to 0$ limit. In Fig. 5(d), we show the ratio of the MSDs for other two values of n_w, with the same findings. Note that the parameters n_w and R enter in the model only through their product [see Eq. (18)]. Hence, the analysis of the dependence of the results on R is not necessary since a change in R at constant n_w is equivalent to a change in n_w at constant R.

It is interesting to see that in all the curves in Figs. 5(a) and 5(b), the convergence to the $\rho(t) \sim t^\alpha$ behavior occurs when $\rho(t) \lesssim 10$ nm. This means that such convergence is determined essentially by the parameters associated to the motors (in particular, k, ϵ, and Π), reinforcing our arguments on the loss of confinement by motors at very small lag times.

A last remarkable fact to observe is that, in the case $\alpha = 1$ shown in Fig. 5(a), for which the dynamics without motors is diffusive, the molecular motors produce subdiffusion at intermediate lag times. Thus, the crosslinking effect of the molecular motors alone enables us to get subdiffusion in a purely viscous medium. The effect is somehow small in the case shown, but it is more notable for smaller values n_w or R (results not shown). It is worth mentioning that the trajectories for $\alpha = 1$ were calculated using the standard Langevin equation coupled to the motor dynamics [33] instead of the Markovian approximation for the overdamped GLE.

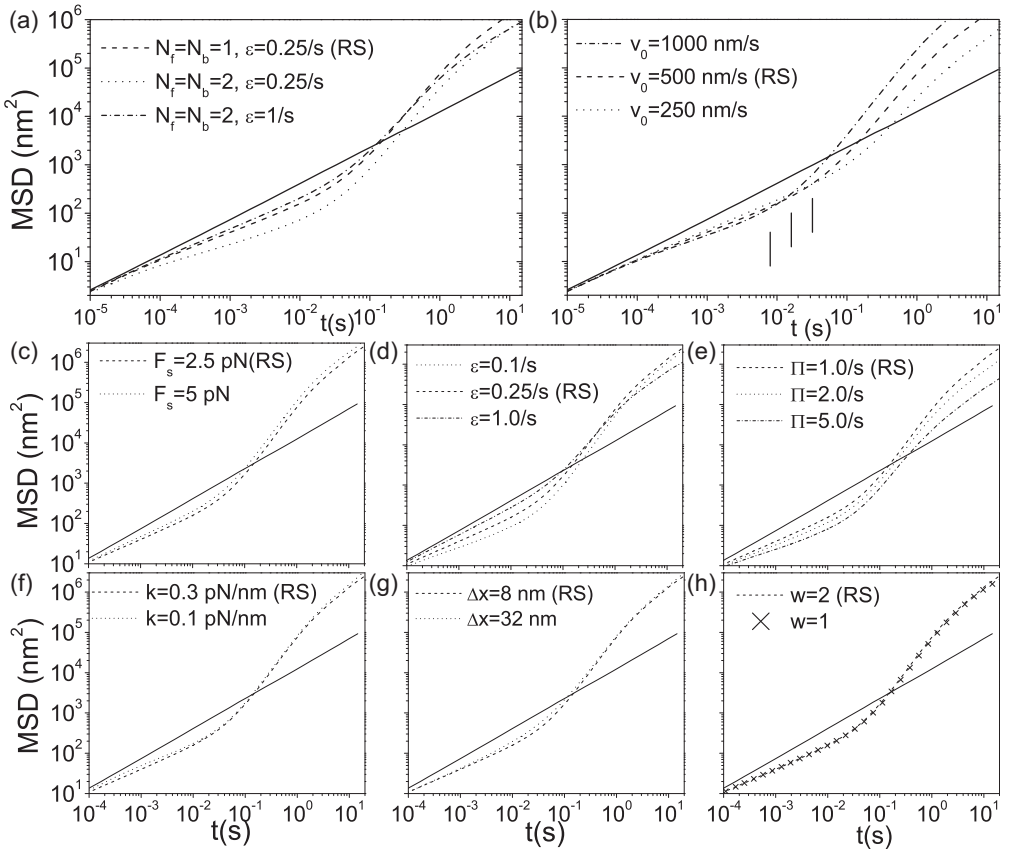

FIG. 4. MSD vs lag time for $a = 0$ considering different parameters for the motor dynamics. For the sake of comparison, in all the panels we include the results for the RS without motors (solid line) and with motors (dashed line). The parameters varied are indicated in each panel, the rest of the parameters for all the curves are those of the RS. In panel (b), the vertical segments indicate the times t_2 where the transition to the superdiffusive regime starts. From left to right, the segments are for $v_0 = 1000$ nm/s, $v_0 = 500$ nm/s, and $v_0 = 250$ nm/s.

C. Relation with experiments

Our results for the transition from subdiffusion to superdiffusion have strong parallels with those found in experiments in [9,10,12–14]. Here, we investigate more deeply the relation of our model to the experiments in [12] while in the Supplemental Material [39] we give a qualitative approach to the experiments in [9]. It is important to indicate that in our approach to the experiments, we only aim at finding good

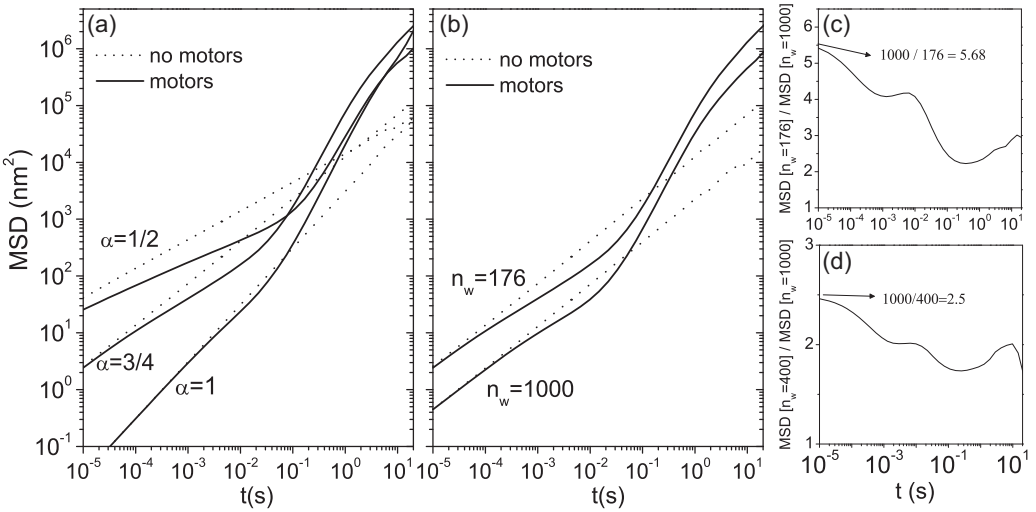

FIG. 5. MSD vs lag time for $a = 0$ considering different parameters for the viscoelastic medium. (a) MSD curves for different values of α with and without motors at fixed $n_w = 176$. (b) MSD curves for different values of n_w with and without motors at fixed $\alpha = 0.75$. (c) The curve corresponds to the MSD for $n_w = 176$ divided by the MSD for $n_w = 1000$. (d) MSD for $n_w = 400$ divided by the MSD for $n_w = 1000$. In all the cases, the parameters that are not indicated in the panels are those of the RS.

qualitative agreement in the correct relevant scales of times and logarithmic slopes. The search for fine tuned curves by varying the system parameters would be meaningless since the model is limited due to its hypothesis of a single power law in $G(\omega)$. Moreover, as we explain later, there are also factors concerning the dimensionality of the system and the winding of the trajectories that should be taken into account for a meaningful fine tuning.

We will show that the experimental data in [12] provide relevant evidence of the action of motors as static crosslinkers reducing the logarithmic slope of the subdiffusive regime as predicted by our model, although this particular point was not discussed in the mentioned reference since the attention was focused on the transition to the superdiffusive behavior. In that work, the authors analyzed myosin V driven transport of melanosomes in frog melanocytes. Microtubules were depolimerized to ensure actin-based transport and two different stimulation conditions called *aggregation* and *dispersion* were studied which correspond to the addition of melatonin and melanocyte stimulating hormone, respectively. Finally, the authors also analyzed transport in cells with mutated myosin V motors that can not attach to actin so that the action of motors is inhibited. The main results in [12] show the existence of a crossover from a subdiffusive to a superdiffusive regime both in cells stimulated for aggregation and dispersion, while only subdiffusive and diffusive behaviors (but not superdiffusive) are found in cells with mutant myosin V.

The authors studied the MSD of the three systems in the ranges of lag time $0.07\ \text{s} \leqslant t < 7\ \text{s}$ [12]. Using a model based on the GLE but in which the motors force is considered as a stochastic noise with a power-law autocorrelation function (i.e., with no model for the motor dynamics), the authors arrived to quite accurate analytical fittings of the local logarithmic slope of the $\rho(t)$ curves of the experimental data in the analyzed region of lag times. The fittings are given by [12]

$$\beta(t) = \frac{d\ \ln[\rho(t)]}{d\ \ln t} = \frac{\frac{\lambda}{\Gamma(\lambda+1)}(t/t_0)^{\lambda} + \varepsilon(2\lambda-\alpha_0)K_{\lambda,\alpha_0}(t/t_0)^{2\lambda-\alpha_0}}{\frac{1}{\Gamma(\lambda+1)}(t/t_0)^{\lambda} + \varepsilon K_{\lambda,\alpha_0}(t/t_0)^{2\lambda-\alpha_0} + \delta}, \quad (20)$$

with $t_0 = 1$ s, $K_{\lambda,\alpha_0} = \Gamma(\alpha_0 - 2\lambda)\{\sin[\pi(\lambda-\alpha_0)] - \sin(\pi\lambda)\}/\pi$, and the set of dimensionless parameters $(\lambda,\alpha_0,\varepsilon,\delta)$ equal to (0.96,0.58,202,41) for aggregation, (0.98,0.58,83,4) for dispersion, and $(0.94,\alpha_0,0,0.061)$ for the mutant system. Note that the value of α_0 is irrelevant for the mutant system given that $\varepsilon = 0$. For an explanation of the meaning of the parameters within the model in [12], see such reference.

In Fig. 6(a), we show the plots of $\beta(t)$ as a function of the lag time t as given by Eq. (20) for the three systems studied in [12]. Note that we consider the time interval where Eq. (20) accurately fits the data of the three experiments and no extrapolation is performed. We see that for small lag times, the logarithmic slope β is larger in the system with inactive (mutant) motors than in the two systems with active motors. In other words, the *activation* of the motors reduces the values of $\beta(t)$ at small t. This is in fact what our model predicts concerning the action of motors as static crosslinkers. The effect in the experiments is particularly notable when comparing the results for mutant motors with those for aggregation, but it is also appreciable in the case of dispersion. Note that the fact that the mutant motors can not link the actin filament implies that these motors can neither act as transport drivers at large t nor as static crosslinkers at small t. Importantly, the present small-t analysis of the experimental curves in [12] is new since in such work the authors focused in the intermediate and large-t regimes.

In order to approach to a description of the experiments in [12] using our model, we have to note first that the consideration of a single power-law behavior for $G(\omega)$ would be an important limitation since the experimental results for mutant motors show a nonconstant value of $\beta(t)$. Nevertheless, we assay an approach focusing on the case of dispersion. We set $\alpha = 0.4$, which is a value in the range that an extrapolation of the $\beta(t)$ curve for the mutant system attain at $t \sim 10^{-2}$ s. Thus, with the action of motors we can expect slopes in the range $\beta \sim 0.5$ or larger for $t \sim 0.1$ s, as those seen in the experiments for dispersion. Importantly, we have to leave the hypothesis of two symmetric teams of motors and consider a single type of motors. For this, we set $N_f = 1$ and $N_b = 0$. We consider an organelle radius $R = 500$ nm as indicated in [12], and all the parameters of the RS excepting for $\epsilon = 0.1/\text{s}, F_s = 2$ pN, and $v_0 = 150$ nm/s. This leads us to the $\beta(t)$ curve shown in dashed lines in Fig. 6(b). We see that it has a quite similar behavior to that of the curve for dispersion shown in panel 6(a), although slightly overestimated. In Fig. 6(b), we also include $\beta(t)$ results for a simulation with two opposing symmetric motors [corresponding to the MSD curve with $\alpha = \frac{1}{2}$ shown in Fig. 5(a)]. The main qualitative difference between systems with symmetric motors and with a single species of motors occurs in the long time regime. We see that for symmetric motors $\beta(t)$ decrease at large t until it reaches values of order $\beta(t) \sim 1$ corresponding the diffusive behavior before discussed. In contrast, for a single type of motors, the superdiffusive behavior is not depleted at long times (at least for $t \sim 10$ s), as it happens in the experiments in [12]. The inset in Fig. 6(b) shows the same curves in the range $10^{-5}\ \text{s} < t < 6\ \text{s}$ where we can see how $\beta(t)$ converge to the corresponding α value at small times ($\alpha = 0.4$ and 0.5 for the dashed and dotted lines, respectively).

D. Organelles in harmonic potentials and a macroscopic approach to the dynamics

Here, we analyze the action of a harmonic potential on a motor-driven organelle. For this, we consider Eqs. (11) with $a \neq 0$ and the force $F_M(x(t),t)$ as given by the motor's stochastic dynamics. The situation may correspond to an optical trapping microrheology experiment as those reported in [35,36]. In our analysis, we consider the harmonic potential $V(x) = ax^2/2$ as extended in the range $-\infty < x < \infty$, so that the organelle would result always confined, independently of the action of motors. It has to be mentioned that in experiments with optical traps, many organelles may escape from the trap due to the action of motors and to the finite size of the trap. For instance, in the experiments in [35], fractions of order 30% or 50% of the organelles escaped in different setups.

In Fig. 7(a), we show the $\rho(t)$ curve considering the parameters in the RS and a harmonic potential with elastic constant $a = 0.02$ pN/nm (solid line). For reference, we also

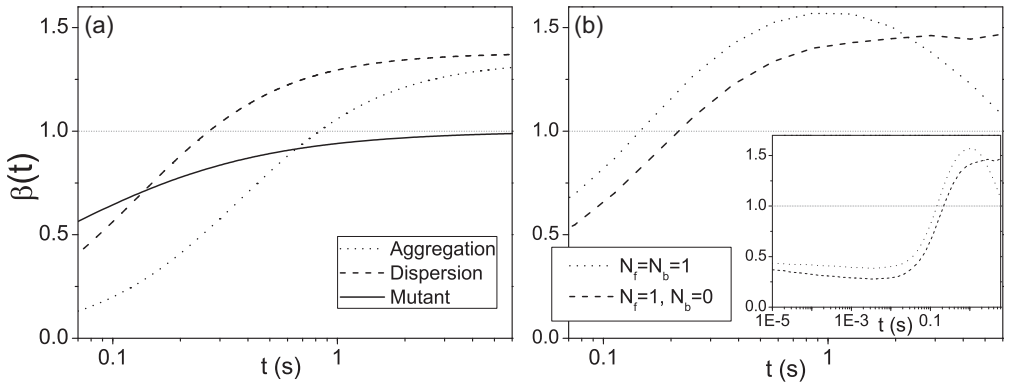

FIG. 6. (a) Fittings for the logarithmic slope $\beta(t)$ of the MSD measured in the experiments in [12]. The curves correspond to the analytic formula given in [12] [Eq. (20) of this paper] with the parameters found in [12] for dispersion, aggregation, and mutant motors. The results show that the logarithmic slope at small lag times grows when the action of motors is inhibited (mutant motors), in agreement with the prediction of our model. (b) Results for $\beta(t)$ from simulations using our model. The dashed line corresponds to simulations with a single type of motors that allow us to approach to the experimental results for dispersion shown in panel (a). The parameters are those of the RS excepting for $\alpha = 0.4, R = 500$ nm, $\epsilon = 0.1/\text{s}, F_s = 2$ pN, and $v_0 = 150$ nm/s. The dotted line corresponds to symmetric motors with parameters as those in the curve with $\alpha = \frac{1}{2}$ in Fig. 5(a). The inset in panel (b) shows the same curves on a wider range of the lag time.

include the curve for $a = 0$ (dashed line) which is the same as that in Fig. 3, and the results for an organelle without motors in the harmonic potential with $a = 0.02$ pN/nm (dotted line). The comparison with the case $a = 0$ indicates that the action of the harmonic potential reduces the time t_1 at which the MSD changes from a $\rho(t) \sim t^{\alpha}$ behavior to a $\rho(t) \sim t^{\beta}$ behavior with $\beta < \alpha$. Moreover, the value of β is reduced, as it changes from $\beta \sim 0.57$ for $a = 0$ (see Fig. 3) to $\beta \sim 0.42$. Finally, the superdiffusive power law is also reduced (from slope 1.7 to 1.2 in this particular case) and a confinement state of constant $\rho(t)$ is found at large t instead of the diffusive regime.

Figure 7(b) shows MSD curves for different harmonic potentials. As expected, excepting for the 0.75 value found at small lag times, all the slopes decrease with a, as well as the asymptotic value of the MSD. In Fig. 7(c), we show the dependence of the asymptotic value of the MSD on the parameter a for two different values of v_0. Interestingly, we find that for small enough elastic constants ($a < 10^{-2}$ pN/nm) the MSD decreases as a^{-1}. This result allows us to provide a macroscopic description for the diffusion by molecular motors in a viscoelastic medium at large lag times. Note that for a system with no motors, the long time MSD value in a harmonic potential is $2k_BT/a$. This is so independently of α and in particular for a pure diffusive system. The fact that we find a^{-1} enables the definition of an effective temperature T_{eff} such that $\rho(t \to \infty) = 2k_BT_{\text{eff}}/a$. Note that such effective temperature is associated to the motors plus cargo plus viscoelastic medium system, and would depend on all the system parameters. In particular, we found $k_BT_{\text{eff}} = 400$ pN nm for the RS and $k_BT_{\text{eff}} = 800$ pN nm for the system with a duplicated value of v_0 analyzed in Fig. 7(c). Thus, the effective temperature seems to be proportional to the velocity of the motors. On the other hand, recalling that for $a = 0$ we find a pure diffusive regime at large times to which we can associate an effective diffusion constant D_{eff} such that $\rho(t) = D_{\text{eff}}\, t$, then, taking into account the relation for pure diffusive media $D = k_BT/\gamma_0$ with γ_0 the friction coefficient [see Eq. (13) with $\alpha = 1$], it is possible to define an effective friction constant γ_{eff} associated to the system given by $\gamma_{\text{eff}} = k_BT_{\text{eff}}/D_{\text{eff}}$. For the RS, we find $\gamma_{\text{eff}} = 3.07 \times 10^{-3}$ pN s/nm. In this way, we obtain a macroscopic simplified diffusive model for the long time dynamics of the cargo-motors system in the viscoelastic medium characterized by the parameters T_{eff} and γ_{eff}. We remark that these two macroscopic parameters may depend on all the system parameters associated to the motors and to the viscoelastic medium but would be independent of the stiffness a of the harmonic potential and of any other external force that could be considered in the system. Note that in the case of nonsymmetric motors, the motion at large time is expected to be biased and thus not purely diffusive so that the macroscopic description just presented should be not valid, as it happens with the system with $N_b = 0$ studied in Fig. 6(b).

The effective temperatures found in our macroscopic description are of order 100 times the absolute temperature, in agreement with the findings in [10]. Such large values of T_{eff} stress the relevance of molecular motors for transport inside cells even in the symmetric motors case where there is no preferred direction of motion [11].

E. MSD in two dimensions

Most of the measurements of the MSD in cell rheology experiments are normally performed on two-dimensional (2D) trajectories $\vec{r}(t) = [x(t), y(t)]$. Thus, instead of the one-dimensional (1D) definition for the MSD given in Eq. (12), we have

$$\Delta r(t)^2 = \frac{1}{N - t/\delta t} \sum_{i=1}^{N - t/\delta t} [x(i\delta t + t) - x(i\delta t)]^2 + [y(i\delta t + t) - y(i\delta t)]^2. \quad (21)$$

To take this into account, we analyze a generalization of our model to two dimensions. Importantly, although we allow the organelle to move in two dimensions, we still consider a straight (not bended) filament where the motors ends (or heads) step.

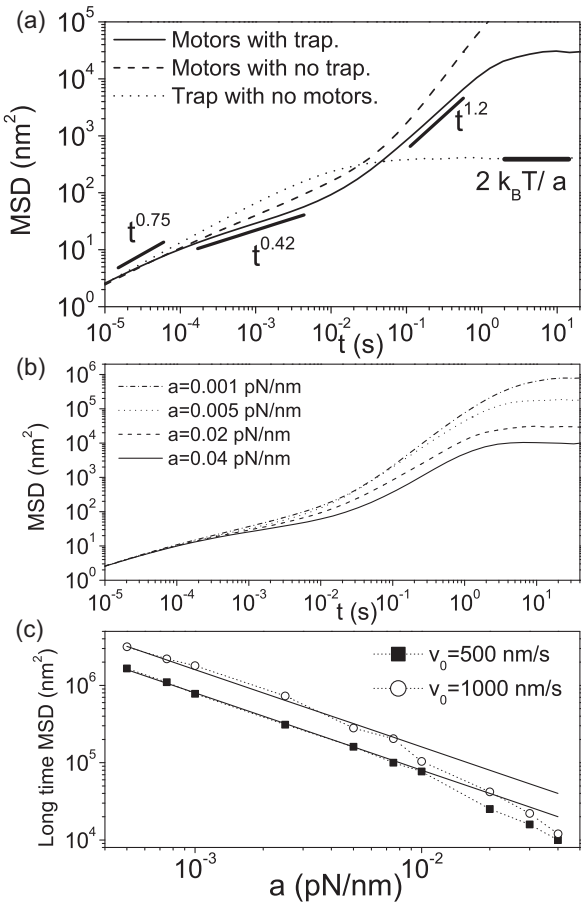

FIG. 7. MSD for organelles in harmonic potentials. (a) Results for the RS considering $a = 0.02$ pN/nm (solid line) and $a = 0$ (dashed line). The dotted line corresponds to $a = 0.02$ pN/nm with $F_M(t) = 0$ (absence of motors). (b) MSD for the RS considering different values of a. (c) Asymptotic value of the MSD as a function of a for two values of the zero load velocity v_0. The solid lines that fit the simulations at small a correspond to 800 pN nm/a for $v_0 = 500$ nm/s and 1600 pN nm/a for $v_0 = 1000$ nm/s. In all the cases, the parameters not indicated in the panels are those of the RS.

We consider the 2D version of Eq. (4) [37]

$$-\int_0^t \gamma(t-t')\dot{\vec{r}}(t')dt' - a\vec{r}(t) + \vec{F}_M(t) + \vec{\xi}(t) = 0, \quad (22)$$

where now the position of the cargo $\vec{r}(t) = [x(t), y(t)]$, the forces and thermal noise are vectorial quantities [37]. Note that the generalization of the Markovian approximation is straightforward. Concerning the model for motors motion, we still consider a one-dimensional filament along the x axis so that the allowed positions for the motor ends on the filaments are of the form $\vec{r} = (j\Delta x, 0)$ with integer j and $\Delta x = 8$ or 32 nm as before. The one-dimensional dynamics for the motors remains the same but now the force exerted on the cargo (at position $\vec{r}$) by a motor at position $\vec{r}_i$ is calculated as $\vec{f}_i = 0$ for $|\vec{r} - \vec{r}_i| \leqslant r_0$ and $\vec{f}_i = -k(|\vec{r} - \vec{r}_i| - r_0)(\vec{r} - \vec{r}_i)/|\vec{r} - \vec{r}_i|$ for $|\vec{r} - \vec{r}_i| > r_0$, with $r_0 = 100$ nm.

In Fig. 8, we compare 2D and 1D results for the MSD considering the parameters of the RS both with and without harmonic potential. It can be seen that at short lag times the

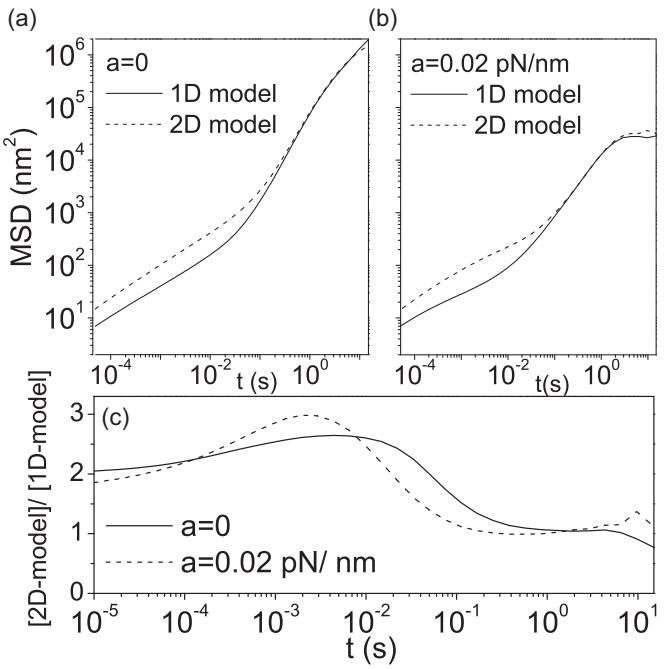

FIG. 8. MSD for the 2D model and comparison with the 1D model. (a) Results with $a = 0$. (b) Results with $a = 0.02$ pN/nm. (c) Ratio between the 2D and 1D MSD curves shown in panels (a) and (b). In all the cases, the parameters are those of the RS.

MSD of the 2D model doubles that of the 1D model, as it is expected for organelles with no motors. Meanwhile, at large lag time both models show essentially the same results since the most relevant displacements are those in the x direction due to the action of the motors. This all shows that the main conclusions found for the 1D system are also valid for 2D systems with straight filaments since one can only expect a modification of the MSD curves by a factor of order 2 at short lag times.

For the case of bended filaments, we also expect changes on factors of order 1 provided that the persistence length of the filaments is larger than the mean length of the forward and backward excursions of the organelles. Note that this condition depends not only on the filament type, but also on the motor types and on the number of motors of each polarity. Another limiting condition for the validness of our model comes from the possibility of an organelle to change the filament on which it is being transported. In the case of microtubule-based transport, this may not be very important since neighbor microtubules are usually almost parallel, but in the case of actin-based transport the effect could be more notable. In any case, the effects of changes of filaments or of bended filaments would be relevant only for long lag times (larger than the typical times between changes on the angle of motion). At such long time scales, the changes of direction would necessarily cause a decreasing of the logarithmic slopes of the MSD curves with respect to those predicted by our models. For instance, note that our model predicts a diffusive behavior at large t only for symmetric motor teams, while nonsymmetric motors lead to superdiffusion at large lag times [as shown in Fig. 6(b)] or even to ballistic average motion (results not shown). However, when random changes of the

angle of motion occur, diffusive motion in 2D can arise in the case of nonsymmetric motors or even for a single type of motors.

IV. CONCLUSIONS AND FINAL REMARKS

We have presented a model based on a generalized Langevin equation (GLE) coupled to a stochastic stepping dynamics for molecular motors that allowed us to analyze important phenomena observed in experiments in cell transport. In particular, the model reproduces transitions from subdiffusive motion at small lag times to superdiffusive motion at large lag times triggered by the action of motors.

The results of our model also indicate that at small lag times, the molecular motors can act as static crosslinkers reducing the logarithmic slopes of the subdiffusive transport in cells with respect to those that would be observed in the absence of motors. Importantly, we have provided a new analysis of the experimental data for transport in frog melanocytes reported in [12] that supports this finding. We have shown that the fittings of the experimental results presented in [12] indicate that the logarithmic slopes of the MSD at small lag times for mutant (inactive) motors are larger than those observed with active motors.

Our approach based on the treatment in [23] considers Eq. (4) as the overdamped limit of the underdamped GLE [Eq. (5)] studied in [23]. This overdamped GLE was also used in [20,35,36] as a model for subdiffusive transport in viscoelastic media. In [39], we show that the main results of the paper can be reproduced considering a more general GLE which includes an additional viscous term [24,25], provided that the corresponding viscosity is small, as expected for cellular systems [25].

We have shown that our general results for the dependence of the MSD on the lag time are rather robust against variations of the parameters defining the motor stepping dynamics. This latter fact suggests that the consideration of more detailed descriptions of the motor's dynamics would not affect our main conclusions. Following the assumptions in [17,29–31], the stochastic stepping dynamics for the motors considered in this paper does not include backstepping. In [32], models with and without back steps have been found to produce very similar results for the force-velocity curves of cargos pulled by multiple motors. The effect of backstepping on the MSD curves is expected to be small, at least clearly much smaller than those produced by the strong variations of the motor parameters analyzed in Fig. 4.

Regarding the influence of the motor dynamics, we have performed an additional check. Note that, in our simulations, an 8-nm motor step occurs in the very small time interval used for the time discretization ($dt \sim 10^{7}$ s), while real motor's steps take more time (typically 10^{-5} s). To take this into account, we considered a modified model (see [39]) in which the probability of a step is ruled by the same Monte Carlo dynamics before introduced, but in which once the algorithm determines the realization of a motor step, the motor step takes a time t_s involving many time discretization steps. During the time t_s, the position of the motor evolves linearly with time at constant velocity 8 nm$/t_s$. The results for the MSD curves obtained with this model are indistinguishable (see [39]) from those found with the original dynamics in the whole range of lag times from 10^{-5} to 10 s, even when we consider t_s as large as 10^{-4} s (i.e., larger than the minimal lag time analyzed). This check provides additional support to our developments, as well as to previous studies of stochastic stepping dynamics for motors coupled to continuous dynamics for cargos in pure viscous environments such as those found in Refs. [30–33].

Finally, we have analyzed the influence of harmonic potentials on the dynamics, and we have discussed the limitations of our model regarding the dimensionality of the system and the possible winding of the organelle trajectories in cells.

ACKNOWLEDGMENT

The author thanks G. Mato for valuable comments, and acknowledges support from CONICET (under Grant No. PIP 112-200801-00076) and from CNEA, both Argentinian agencies.

[1] J. Howard, *Mechanics of Motor Proteins and the Cytoskeleton* (Sinauer Associates, Sunderland, MA, 2001); R. Vale, Cell **112**, 467 (2003).
[2] M. A. Welte, Curr. Biol. **14**, R525 (2004); S. P. Gross, Phys. Biol. **1**, R1 (2004).
[3] C. Desnos, S. Huet, and F. Darchen, Biol. Cell **99**, 411 (2007).
[4] M. Y. Ali *et al.*, Proc. Natl. Acad. Sci. USA **108**, E535 (2011).
[5] D. Wirtz, Annu. Rev. Biophys. **38**, 301 (2009).
[6] T. A. Waigh, Rep. Prog. Phys. **68**, 685 (2005).
[7] T. G. Mason and D. A. Weitz, Phys. Rev. Lett. **74**, 1250 (1995).
[8] F. Gittes and F. C. MacKintosh, Phys. Rev. E **58**, R1241 (1998).
[9] K. M. Van Citters *et al.*, Biophys. J. **91**, 3946 (2006).
[10] F. Gallet, D. Arcizet, P. Boheca, and A. Richerta, Soft Matter **5**, 2947 (2009).
[11] C. P. Brangwynne *et al.*, Trends Cell Biol. **19**, 423 (2009).
[12] L. Bruno, V. Levi, M. Brunstein, and M. A. Despósito, Phys. Rev. E **80**, 011912 (2009).
[13] H. Salman, Y. Gil, R. Granek, and Me. Elbaum, Chem. Phys. **284**, 389 (2002).
[14] P. Bursac *et al.*, Nat. Mater. **4**, 557 (2005).
[15] R. Lipowsky *et al.*, Phys. E (Amsterdam) **42**, 649 (2010); M. J. I. Müller, S. Klumpp, and R. Lipowsky, Biophys. J. **98**, 2610 (2010).
[16] F. Berger, C. Keller, S. Klumpp, and R. Lipowsky, Phys. Rev. Lett. **108**, 208101 (2012).
[17] A. Kunwar *et al.*, Proc. Natl. Acad. Sci. USA **108**, 18960 (2011).
[18] W. Nam and B. I. Epureanu, J. Phys.: Condens. Matter **24**, 375103 (2012).
[19] J.-D. Bao, Y.-Z. Zhuo, F. A. Oliveira, and P. Hänggi, Phys. Rev. E **74**, 061111 (2006).
[20] S. C. Kou, Ann. Appl. Stats **2**, 501 (2008).
[21] A. D. Viñales, K. G. Wang, and M. A. Despósito, Phys. Rev. E **80**, 011101 (2009).
[22] M. A. Despósito and A. D. Viñales, Phys. Rev. E **80**, 021111 (2009); A. D. Viñales and M. A. Despósito, *ibid.* **75**, 042102 (2007).

[23] I. Goychuk, Phys. Rev. E **80**, 046125 (2009).
[24] I. Goychuk, Adv. Chem. Phys. **150**, 187 (2012).
[25] I. Goychuk, V. O. Kharchenko, and R. Metzler, PLoS ONE **9**, e91700 (2014).
[26] I. Goychuk, V. O. Kharchenko, and R. Metzler, arXiv:1312.5526.
[27] I. Goychuk, Chem. Phys. **375**, 450 (2010).
[28] V. Kharchenko and I. Goychuk, New J. Phys. **14**, 043042 (2012).
[29] G. T. Shubeita *et al.*, Cell **135**, 1098 (2008).
[30] A. Kunwar, M. Vershinin, J. Xu, and S. P. Gross, Curr. Biol. **18**, 1173 (2008).
[31] A. Kunwar and A. Mogilner, Phys. Biol. **7**, 016012 (2010).
[32] S. Bouzat and F. Falo, Phys. Biol. **7**, 046009 (2010).
[33] S. Bouzat and F. Falo, Phys. Biol. **8**, 066010 (2011).
[34] S. Bouzat, V. Levi, and L. Bruno, PloS One **7**, e43599 (2012).
[35] E. Bertseva *et al.*, Eur. Phys. J. E: Soft Matter Biol. Phys. **35**, 63 (2012).
[36] D. S. Grebenkov, M. Vahabi, E. Bertseva, L. Forró, and S. Jeney, Phys. Rev. E **88**, 040701(R) (2013).
[37] A. W. C. Lau, B. D. Hoffmann, A. Davies, J. C. Crocker, and T. C. Lubensky, Phys. Rev. Lett. **91**, 198101 (2003).
[38] E. Helfand, Bell Syst. Tech. J. **58**, 2289 (1979).
[39] See Supplemental Material at http://link.aps.org/supplemental/10.1103/PhysRevE.89.062707 for detailed description of numerical methods and relation with other models.
[40] J.-H. Jeon and R. Metzler, Phys. Rev. E **85**, 021147 (2012).
[41] V. Levi, V. I. Gelfand, A. S. Serpinskaya, and E. Gratton, Biophys. J. **90**, L07 (2006).
[42] M. J. Schnitzer, K. Visscher. and S. M. Block, Nat. Cell Biol. **2**, 718 (2000); N. J. Carter and R. A. Cross, Nature (London) **435**, 308 (2005).
[43] P. A. Sims and X. S. Xie, Chem. Phys. Chem. **10**, 1511 (2009).